Elucidating the role of hydrogen bonds for improved mechanical properties in high-performance semiconducting polymer

Luke A. Galuska[1‡], Michael U. Ocheje[2‡], Zachary C. Ahmad[1], Simon Rondeau-Gagné[2*], Xiaodan Gu[1*]

[1]Center for Optoelectronic Materials and Devices, School of Polymer Science and Engineering, the University of Southern Mississippi, Hattiesburg, MS 39406, USA.

[2]Department of Chemistry and Biochemistry, University of Windsor, Advanced Materials Centre of Research, Windsor, ON, Canada N9B3P4.

[‡]These authors contributed equally to this work.

ABSTRACT: Incorporation of hydrogen bond moieties into the backbone or side chain of conjugated polymers is an effective strategy to enhance mechanical performance, facilitate morphological organization, and promote self-healing ability. However, the understanding of hydrogen bonds, particularly the effect of bond strength and directionality, on thermomechanical and optoelectronic performance is still in its infancy due to the competing influence of morphology, glass transition phenomena, and the measurement process itself. Here, we compare the influence of statistically incorporated amide and urea moieties on the mechanical properties of DPP-TVT parent polymers. We observed a profound difference in ductility; amide functionalization increases the strain at failure by over 100% relative to pure DPP-TVT polymer, while urea functionalization results in a loss of strain at failure by 50%. This is attributed to the crystalline behavior of functionalized conjugated polymers that is promoted by intermolecular interactions of urea groups, which we elucidated via an in-depth investigation of the swelling, crystalline packing, thermal behavior, and strain dependent charge transport. Furthermore, we employed a novel free-standing tensile test to validate our mechanical measurements supported on a water surface. Our results demonstrated that hydrogen bond moieties must be carefully chosen to achieve a delicate balance of morphological control and mechanical performance, as simply increasing the hydrogen bond strength can result in detrimental mechanical and electrical performance.

Introduction

Electronics are getting more interconnected and integrated to everyday objects through flexible and conformable devices in order to grow an expansive quantity of data, the interest and need for mechanically robust materials has been steadily increasing.[1–7] As improved mechanical properties result in devices with increased lifetimes, new materials are currently being developed to confer emerging electronics with the ability to be incorporated into (and onto) more complex topographies. Among the different electroactive materials that can be used to fabricate and develop stretchable/flexible electronics, organic π-conjugated polymers are particularly promising. Compared to their inorganic counterparts, these organic semiconductors have the advantage of possessing superior thermomechanical properties that can easily be modified and enhanced even further.[8–11] Recent π-conjugated polymers have also been shown to possess good charge transport and the possibility of being deposited in solution, opening new avenues for the large-scale manufacturing of soft electronics.

Many strategies have been implemented by researchers to develop semiconducting polymers capable of accommodating large strains and with favorable thermomechanical properties.[12–14] One popular method is to blend the semiconducting material with soft and stretchable elastomers. Many recent examples focus on this physical blending with poly(dimethylsiloxane) (PDMS), styrene-ethylene-butadiene-styrene (SEBS), polyethylene (PE), or butyl rubber (BR) to control and improve the thermomechanical properties of rigid semicrystalline semiconducting polymers, principally occurring through a nanoconfinement of the conjugated polymer chains in a soft matrix.[15–20] This method is straightforward, but comes with the inherent disadvantage of introducing insulating material into the active layer of an electronic device.

To circumvent this drawback, strategies for the synthesis of intrinsically stretchable conjugated polymers through precise molecular engineering have been explored in the recent literature.[21–24] Performed through the insertion of bulky soft side chains or through the utilization of conjugation breaking units, the molecular design of π-conjugated polymers is an effective approach to generate materials with increased amorphous content, reduced crystallinity and improved resistance to mechanical failure all while maintaining good charge transport properties. One particularly promising approach to generate intrinsically stretchable semiconducting polymers with new properties is through the utilization of dynamic supramolecular interactions. Non-covalent interactions, either inserted on the polymer's side chains or backbone, have been shown to significantly impact the polymer solid-state morphology and to help tensile strain dissipation and chain alignment upon strain. Among the different types of noncovalent interactions used in semicrystalline conjugated polymers, hydrogen bonds have been especially investigated. For example, Oh *et al.* implemented a backbone engineering approach by synthesizing and incorporating a pyridine dicarboxamide (PDCA) moiety as a conjugation-break spacer into DPP-based

polymers.[25] Although the charge mobility decreased slightly with increasing incorporation of these non-conjugated segments, the novel polymers still exhibited high stretchability as well as high conductivity, achieving a hole mobility of greater than 0.1 $cm^2V^{-1}s^{-1}$ while being stretched to 100% elongation and demonstrated their viability in fully functional, fully-stretchable devices. In a similar manner, Gasperini *et al.* expanded on this work by instead using the PDCA unit in side-chain engineered DPP polymers.[26] Through extensive characterizations, they showed that the location and the amount of hydrogen-bonding units in conjugated polymers have an important influence on the thermal and mechanical properties. Finally, hydrogen bonding has been shown to lead to particularly impressive charge transport values in organic field-effect transistors (OFETs).[27,28]

Although the use of hydrogen bonds to dissipate tensile strain is a strategy that has been employed to great effect, some challenges remain to fully unveil and predict their influence on the optoelectronic and thermomechanical properties of high-performance semiconducting polymers. First, only a relatively low content of hydrogen-bonding moieties (typically between 10-20 mol%) can be typically incorporated in semiconducting polymers through side chain engineering to avoid a drastic reduction of the polymer solubility, which makes a direct observation and quantification of the effect of these hydrogen bonds on the thermomechanical properties rather challenging. Moreover, most techniques used to evaluate the thermomechanical properties of conjugated polymers in ultrathin films rely on support (elastomer or water), which can influence the formation of intermolecular hydrogen bonds. Finally, the effect of moisture on these materials in the solid-state is still not well known and difficult to control.

Herein, an in-depth characterization of semiconducting polymers incorporating urea and amide moieties allowing for intermolecular hydrogen bonding is performed to fully unravel the impact of hydrogen bonds on the optoelectronic and thermomechanical properties of semicrystalline π-conjugated polymers. A careful investigation of the effect of water molecules on hydrogen-bond functionalized DPP-based conjugated polymers is also performed by using a shear motion-assisted robust transfer method for fabricating free-standing ultrathin films, thus allowing for the direct observation and quantification of the effect of water on the mechanical properties of intermolecularly hydrogen-bonded films. Our work suggests that hydrogen bonding strength alone is not a good indicator of mechanical performance. The resulting influence on crystalline packing plays a significant role in performance and may out way any benefit provided via energy dissipation of hydrogen bonds.

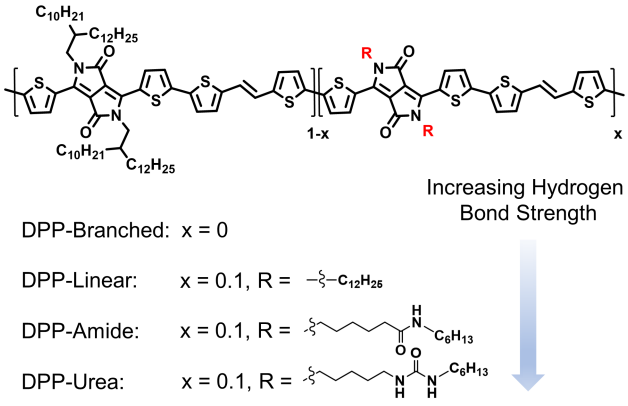

Figure 1: Chemical structures of DPP-TVT based conjugated polymers investigated in this study.

Mechanical analysis via supporting mediums

Here we discuss the thin film mechanics of four DPP-TVT based polymers (Figure 1 and Table 1). The polymers consist of DPP-TVT copolymer and three statistical copolymers with either linear alkyl, amide, or urea moieties incorporated at 10 mol% ratio in the sidechains. Detailed synthesis of those four polymers can be found in the supporting information. These alterations to the DPP-TVT parent polymer have three primary modes of influence, namely 1) Interfacial interaction with supporting medium, 2) morphological changes and particularly to the crystalline domain and 3) chain dynamics or the glass transition phenomena, all of which dictate mechanical performance.

We note that there are several factors that should be carefully evaluated to compare the mechanical property of hydrogen-bonded conjugated polymers. Firstly, when dealing with ultra-thin films it is paramount to understand how the measurement process dictates the observed mechanical properties. The supporting interface may either stiffen or soften a polymer film depending on their interaction.[29] As this work relies on water as a support, increased hydrogen bonding may result in plasticization at the film-water interface and lead to a reduced modulus. However, this is unexpected for the measurement as the concentration of hydrogen bonding moieties is limited to 10 mol% incorporation and the contact time with water is less than 5 minutes.

Table 1: Polymer material and mechanical properties

Polymer	M_n(kDa)	Đ	E (MPa)	SAF[b]	COS[c]
Branched	29.0	3.1	$380.7_{(21.9)}$[a]	$0.10_{(0.03)}$	N/A
Linear	31.4	4.2	$416.7_{(5.4)}$	$0.09_{(0.01)}$	0.25
Amide	35.7	2.1	$357.4_{(18.5)}$	$0.22_{(0.02)}$	0.5
Urea	31.3	1.8	$371.6_{(7.4)}$	$0.05_{(0.01)}$	0.5

[a] Standard deviation from a minimum of four individual tensile measurements. [b] Abbreviation for strain at failure. [c] Abbreviation for crack onset strain.

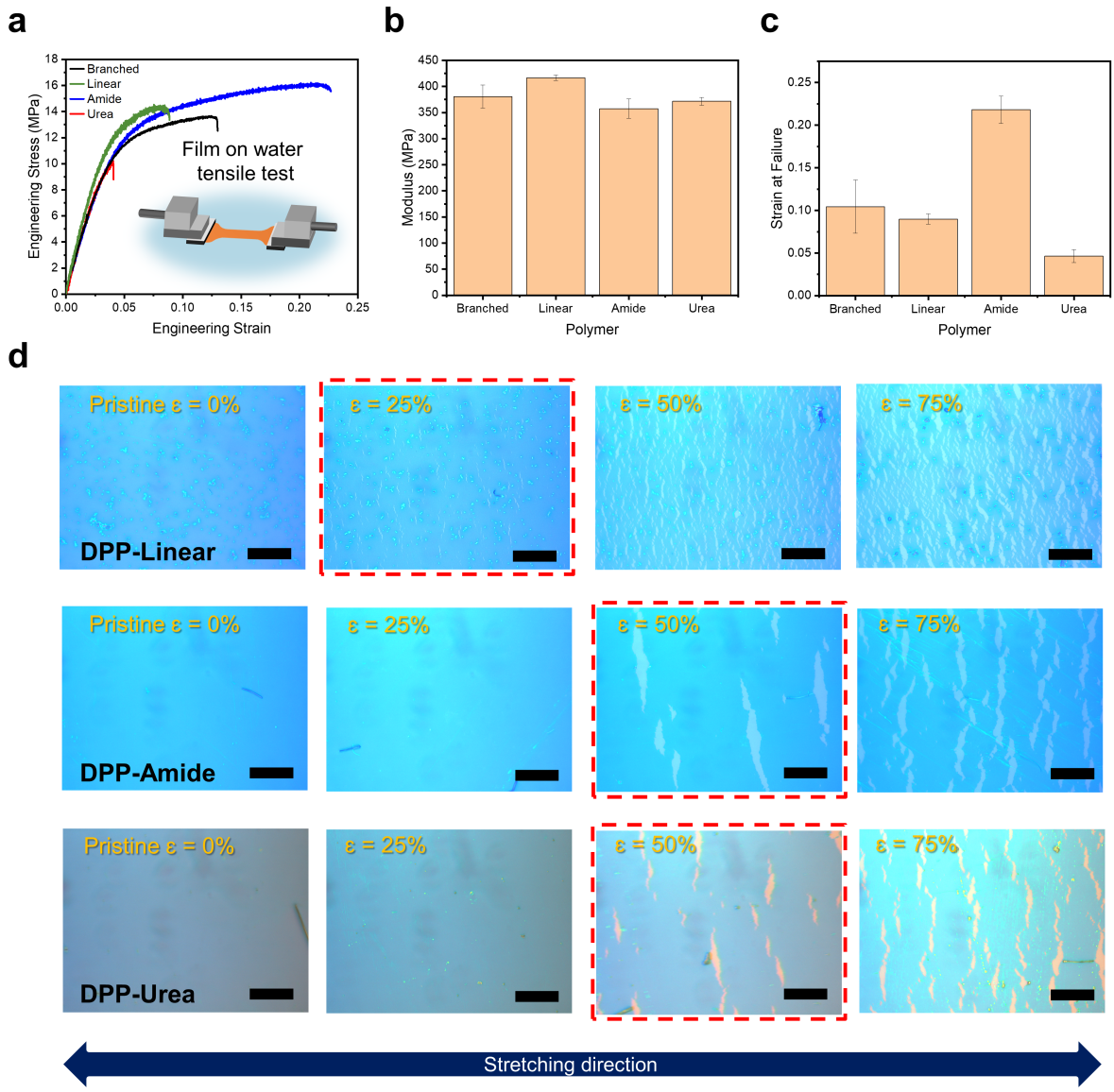

Figure 2: Thin film mechanical properties as measured by the film-on-water and film -on -elastomer techniques. (a) Representative stress-strain plots of DPP-TVT-based polymers. Insert is an illustration of the film on water tensile measurement. (b) Modulus of each polymer measured in the standard film-on-water process. (c) Strain at failure of each polymer measured in the standard film-on-water process. (d) Representative optical images of the three statistical copolymers strained via the film on elastomer technique. The dashed red outline indicates the crack onset strain for each polymer. Scale bar is 25 microns. Error bars represent the standard deviation of the data.

Secondly, statistical copolymers are likely to have reduced modulus as random incorporation disrupts the crystalline packing behavior resulting in increased amorphous content.[30–32]The intermolecular interactions of hydrogen bonding may further disrupt or promote the packing behavior, as previously observed for amide and urea incorporation, respectively.[27,33] Lastly, hydrogen bonding is expected to increase the glass transition temperature (T_g), reducing the conformational freedom of the system, resulting in increased modulus. Additionally, H-bonding offers additional routes for energy dissipation which may increase ductility.

The film-on-water tensile test was first used to assess the mechanics of these polymers in the thin film state. This technique can be found in our recent review article.[29] Figure 2a shows representative stress-strain profiles for each polymer under an applied strain rate of $5*10^{-4}s^{-1}$. All polymers demonstrate similar elastic modulus with a trend in average modulus as follows: DPP-Linear > DPP-Branched > DPP-Urea > DPP-Amide > (Figure 2b). The increased modulus for DPP-Linear over the branched counterpart was expected given the reduced side chain content which acts as an internal plasticizer.[34] Interestingly, DPP-Amide and DPP-Urea demonstrated a lower modulus than DPP-Linear despite their ability to form hydrogen bonds which would result in

an increased T_g. This implies that either the influence of water or their crystalline structure may be responsible for the reduced modulus. In terms of DPP-Amide and DPP-Urea, their modulus agrees with the expected trend in hydrogen bond strength. The strength of hydrogen bonding can be quantified by the hydrogen bonding cohesion parameter which is 25.5 $(J/cm^3)^{1/2}$ and 34.2 $(J/cm^3)^{1/2}$for amide and urea moieties respectively.[35] The difference in ductility of these films was pronounced (Figure 2c). DPP-Amide demonstrated the highest strain at failure of 22% followed by DPP-Branched at 10%, DPP-Urea at 5%, and DPP-Linear at 3%. This was quite interesting as DPP-Urea exhibited poor ductility despite having the greatest hydrogen bonding strength.

One question that emerges is the influence of water on the previous film-on-water tensile test, as increased hydrogen bonding moieties may result in plasticization by the water support. In our previous work DPP-Amide was observed to have a lower modulus than DPP-TVT attributed to reduced crystallinity.[33] The same trend in modulus was observed for both the film-on-water technique and nanoindentation. This indicates plasticization by water is not the reason for the reduced modulus in the statistical copolymers relative to DPP-Branched.

To explore this further, we performed two additional thin film tensile measurements to preferentially exclude or exacerbate the interaction of the hydrogen bonds with the supporting media. First, tensile measurements using the film-on-elastomer method were used to assess the ductility of each polymer (Figure 2d). In this method the potential energy dissipation provided by the hydrogen bonds should be fully available resulting in extended ductility. Like the film-on-water measurement, the crack onset strain (COS) was greatest for DPP-Amide, with an even greater value of ~ 50% strain. In contrast to the film-on-water measurement, DPP-Urea exhibited increased ductility, like that of DPP-Amide, which was attributed to the energy dissipation provided by the urea moieties. Second, we kept each polymer film on water for a period of 24 hours prior to tensile testing (Figure S1a). All the polymers exhibited a reduction in modulus, and this was most dramatic in the case of DPP-Amide films (Figure S1b). DPP-Amide exhibits a 34% reduction in modulus while DPP-Urea, DPP-Branched, and DPP-Linear exhibit a 23%, 20%, and 28% reduction respectively. Despite the reduction in modulus, DPP-Amide exhibits near identical strain at failure relative to the conventional film-on-water method (Figure S1c). Given that the hydrogen bonds are likely disrupted by the presence of the water, as evidenced by the reduced modulus, it is unlikely that energy dissipation via hydrogen bond disassociation is solely responsible for the high ductility of DPP-Amide. Rather, we surmise that the full impact of these hydrogen bonds lies within the initial film formation through disruption of the crystalline morphology and promotion of amorphous entanglements. In contrast, DPP-Urea exhibited both low and high ductility depending on the measurement condition. This indicates two competing mechanisms which dictate its mechanical performance, that is, energy dissipation via hydrogen bonding (increasing ductility) and potentially high crystallinity (reducing ductility). In the case of the film-on-water measurement, hydrogen bonds were disrupted resulting in crystallinity dictating the films ductility.

To further elucidate the mechanism by which hydrogen bonding influences the mechanics, we explored the free-

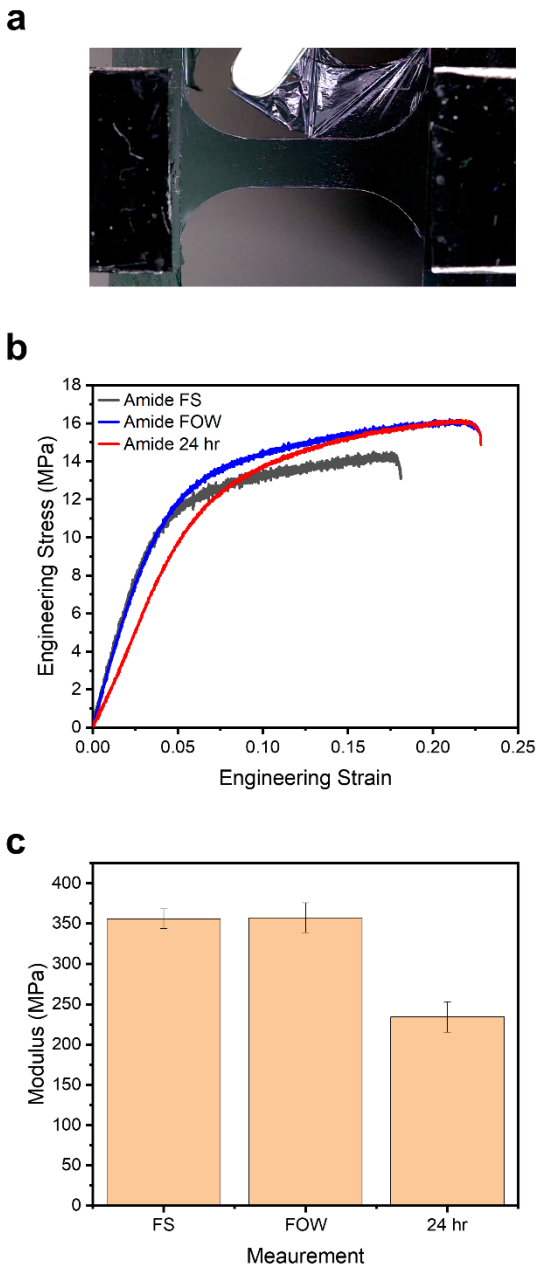

Figure 3: Free-standing tensile measurement and comparison with the film on water techniques. (a) Optical image of a free-standing (in air) DPP-Amide 80nm film with side supports being removed prior to the tensile measurement. (b) Representative stress-strain plots comparing the three tensile measurements for DPP-Amide. (c) Modulus comparison of DPP-Amide films measured in the free-standing environment, film on water, and after prolonged exposure to water.

standing mechanics, followed by the swelling behavior, morphology characterization with an emphasis on the crystalline packing, glass transition temperature, and strain dependent charge transport.

Free-standing Measurements

To assess the water molecule's potential influence on the mechanical properties we performed fully free-standing tensile measurements of DPP-Amide. The general exposure time during the film-on-water method is approximately 5 minutes, where the water could impact thin film mechanics. The free-standing films (in air) were obtained via the shear motion assisted robust transfer method (SMART) outlined in our previous publication.[36] DPP-Amide, 80 nm in thickness, was successfully transferred and measured using the SMART technique (Figure 3a and Movie S1). DPP-Urea was also attempted but failed due to its brittle nature and limited thickness (Movie S2). Figure 3b shows the representative stress-strain profile of DPP-Amide obtained from the free-standing tensile tests relative to the film-on-water and post 24-hour measurements. The modulus was observed to be identical for the free-standing and film-on-water methods (Figure 3c) while the strain at failure was reduced. Such a trend was previously observed for free-standing polystyrene films and attributed to a crack mitigation mechanism provided by the water interface.[36,37]

Swelling Measurement

The swelling of polymer films was assessed over a 24-hour period using *in situ* ellipsometry in an aqueous environment (Figure 4a). In this experiment, we spin coated conjugated polymers onto silicon substates with a 500nm silicon dioxide layer and sealed the film in a liquid cell filled with deionized water and monitored film thickness change continuously. Ellipsometry uses two components of polarized light, Ψ and Δ, to obtain high sensitivity to film thickness and optical constants. Ψ is the ratio of the amplitude change of the polarized light while Δ is the phase difference. Representative raw data for Ψ is shown in Figure 4b for DPP-Amide. There is a slight red shift of the data from 0 to 24 hours which indicates a small increase in thickness. The raw Ψ and Δ data were successfully fitted using an anisotropic model consisting of a series of gaussian oscillators to appropriately model the data with low mean square error (MSE) and statistically unique thickness (Figures S2a).[38] The modeled thickness profiles for each polymer film are shown in Figure S2b. We observed a notable difference in swelling behavior with increased hydrogen bond strength (Figure 4c). DPP-Branched exhibited low swelling over 24 hours and had the slowest initial swelling rate. This indicates that the interaction between DPP-Branched, and water was relatively limited. Linear DPP has an accelerated swelling rate and plateaus with a swelling of 2.8%. Such an increase in the swelling behavior can be attributed to the relative increase of carbonyl functionality as the side chain content is reduced from the branched to linear motif. DPP-Amide exhibited the highest swelling of 3.5% and demonstrated a high initial swelling rate. In contrast, DPP-Urea has the most

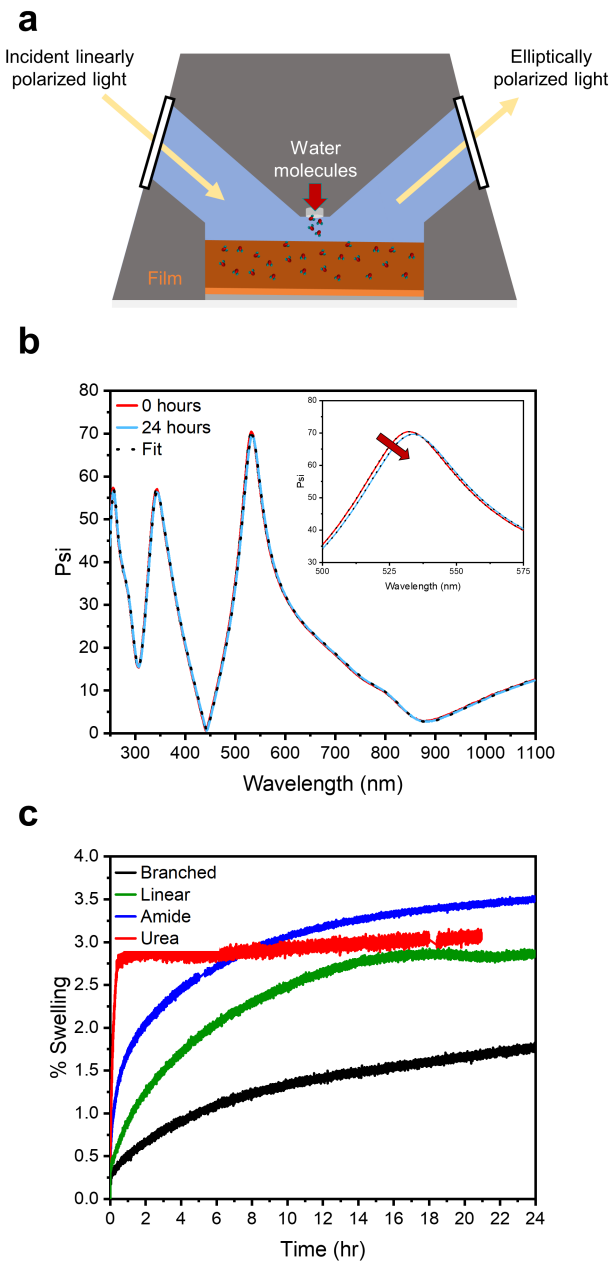

Figure 4: Thin film swelling as measured by ellipsometry in an aqueous environment. (a) Illustration of the liquid cell measurement to monitor film water uptake. (b) Comparison of the raw Psi data for DPP-Amide upon initial water contact and after 24 hours. The insert demonstrates the red shift of the Psi peak at ~ 530 nm indicating a small increase in thickness. (c) Percent swelling occurring in each film throughout 24 hours of exposure to a water environment at room temperature.

rapid initial swelling, but plateaus in less than 1 hour. The initial rapid swelling by DPP-Urea is attributed to the stronger hydrogen bond interaction of urea moieties with water. It has been observed that upon addition of water, urea dimers are destroyed due to the preferential association between urea and water.[39] Given that our tensile measurement requires approximately five minutes of exposure

of the film to water, DPP-Urea would exhibit over half of its swelling in this time. Thus, such a rapid initial swelling may result in plasticization leading to the reduced modulus exhibited by DPP-Urea in the film-on-water tensile test. The plateau in the swelling of DPP-Urea indicates that there are no more urea moieties assessable to the water. This seems counterintuitive as we would generally expect a greater degree of swelling to occur given the increase in hydrogen bonding functionality. However, the inclusion of urea moieties has been known to promote crystallization in DPP-based polymers which would decrease the available urea moieties for plasticization as the penetration of water into such crystalline regions may be diffusion limited.[27] This hypothesis agrees with our mechanical property observations in that DPP-Amide shows not only greater ductility than DPP-Urea but also a more dramatic reduction in modulus upon extended exposure to water, both of which may be attributed to reduced crystallinity. Additionally, we were able to extract the thin film optical constants throughout the swelling process (Figure S2c). There is negligible change to the absorption profile of these polymers even after 24 hours of exposure to water. This indicates that plasticization of water does not significantly influence the conjugated polymer backbone but lies solely on the side chain as is expected. It is also worth noting, all the polymers studied here consisted mostly of branched alkyl sidechains, thus rendering a hydrophobic film. Thus, all the films showed limited swelling which is in agreement with previous neutron reflectivity data for thin film floated on a water surface.[36]

Influence of hydrogen bonding on morphology and dynamics

The crystalline packing of each polymer film was assessed through grazing incidence wide angle X-ray scattering (GIWAXS). All polymers exhibited similar alkyl and π-π scattering peaks with D-spacings on the order of 22Å and 3.6Å, respectively (Figure S3-4 and Table S1-2). This is not unexpected as the only difference lies in the statistically incorporated side chain moieties at 10% concentration. What does change however is the orientation of the crystalline packing and the relative degree of crystallinity (rDoC). The crystalline orientation is primarily edge-on for DPP-Branched, DPP-Linear, and DPP-Urea, while DPP-Amide exhibits a more isotropic orientation. To further assess the packing behavior, we performed a pole figure analysis of the (200) scattering peaks to obtain the rDoC of each polymer.[40,41] The rDoC is highly related to the mechanical performance of the films whereby a higher rDoC would be expected to yield a higher modulus and reduced ductility. Relative to pure DPP-Branched, with an assigned rDoC of 1, DPP-Linear and DPP-Urea observed an increase in the rDoC to 1.18 and 1.48 respectively. In contrast, DPP-Amide demonstrated a reduction in the rDoC to a value of 0.95 (Figure 5). The trend in rDoC strongly matches the ductility of these polymers. For example, DPP-Amide and DPP-Branched exhibited the highest ductility's yet have the lowest rDoC values. The trend in modulus matched that of the rDoC for all the polymers expect DPP-Urea which exhibited the highest rDoC yet possessed a reduced modulus relative to DPP-Branched and DPP-Linear. This further confirms the plasticization of DPP-Urea by water molecules.

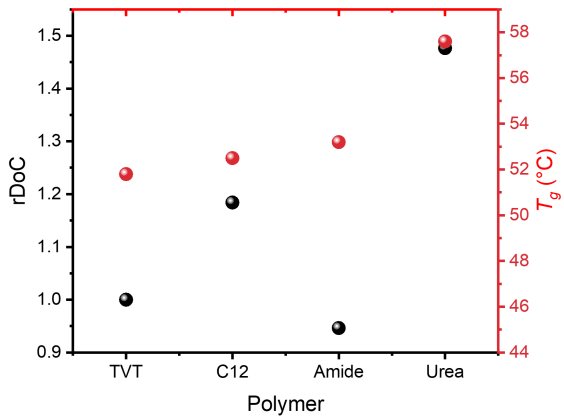

Figure 5: Relative degree of crystallinity and glass transition temperature of each polymer measured by GIWAXS and temperature dependent ellipsometry respectively.

We further asses the crystalline packing of each film by exposure to water for 24 hours followed by GIWAXS measurement in the dry state (Figure S3-4 and Table S1-2). The purpose was to determine if there was any influence of the water on the crystalline nature of these films. We observed an increase in the rDoC of these films which decreased with increasing hydrogen bond strength. DPP-Urea exhibited the only reduction in rDoC. The change in rDoC was attributed to plasticization by water over the 24 hr exposure period. This further supports the previous trends in mechanics and swelling behavior.

Glass transition temperature is a primary parameter which governs conjugated polymer mechanical performance. As T_g increases modulus increases resulting from the restriction of chain dynamics, which, may in turn also reduce the ductility of the system.[24,34,42,43] Here an increase in T_g is expected with increasing hydrogen bond strength. We elucidated the T_g of these polymers through temperature dependent ellipsometry, whereby a discontinuity in the thermal expansion (thickness), as the films are heated at a constant rate, is indicative of the T_g (Figure 5 and Figure S5).[44–46] The polymers observed a clear trend in T_g as follows: DPP-Urea > DPP-Amide > DPP-Linear > DPP-Branched. It is important to note, that the change in T_g for the polymers is relatively low compared to the rDoC and thus we conclude that the crystalline packing dominated the observed mechanical performance and in particular the strain at failure.

Strain Dependent Charge Transport

OFET devices were fabricated to assess the charge transport dependence on strain (Figures 6 and S6-9). At 0% strain the charge mobility was 0.148, 0.199, and 0.0154 cm^2/Vs for DPP-Linear, DPP-Amide, and DPP-Urea respectively. The charge mobility was further assessed parallel and perpendicular to the strain direction up to 75% strain.

DPP-Urea demonstrated the greatest reduction in charge transport upon applied strain, with a 94% reduction in charge mobility at 25% strain in the parallel configuration. Regarding the previous FOE measurements this is quite interesting as the COS for DPP-Urea was equivalent to that of DPP-Amide. This indicates that the charge pathways were easily broken upon applied strain in DPP-Urea, prior to visible crack formation. In contrast, the charge transport of DPP-Amide decayed only 14% at 25 % strain. Considering the typical maximal strain experienced by human skin is 33%, amide functionalization may be a suitable synthetic strategy to achieve the tolerable strain for wearable devices while maintaining charge transport. These results indicate that the greater hydrogen bonding strength of the urea moiety was not advantageous as an energy dissipation mechanism, but rather detrimental due to the promotion of crystallite formation.

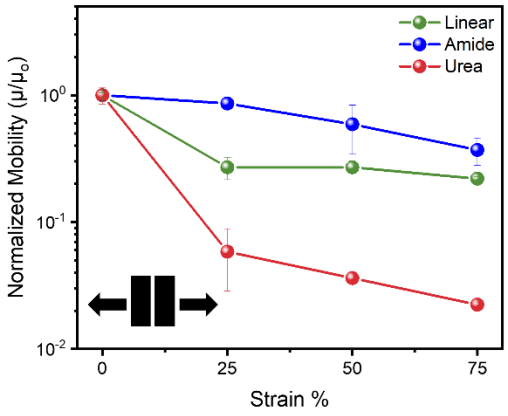

Figure 6: Strain dependence on the normalized mobility of the statistical copolymers in the parallel to strain direction.

Conclusion

In summary, three DPP-TVT based statistical copolymers (with 10% linear alkyl side chain, amide functional sidechains, and urea functional sidechains) were assessed relative to DPP-TVT with branched sidechains to elucidate the role of hydrogen bonding on thin film mechanics. Amide and urea moieties demonstrated strikingly different effects, with amide functionalization yielding the highest ductility while urea functionalization resulted in embrittlement of the polymer. This is attributed to the diverging influence on crystalline packing. Amide functionalization disrupts crystallite orientation resulting in a highly beneficial response to tensile deformation, while urea incorporation results in directed crystallization and an inability to accommodate stress. This was further assessed by characterization of the polymer swelling behavior, whereby, DPP-Amide exhibited the greatest swelling of 3.5% after prolonged exposure, indicating the greater availability of amide moieties for interaction with water resulting from the disruption of crystalline packing. In contrast DPP-Urea possessed an initially rapid swelling behavior, but quickly plateaued due to the greater crystallinity. We further validated our film-on-water measurements by performing a free-standing tensile characterization of DPP-Amide, using our SMART technique, which exhibited identical modulus to the film-on-water technique. This indicates that the polymers must be exposed for prolonged periods in water (e.g., tens of hours) for water plasticization effect to occur. To conclude, hydrogen bond moieties offer a novel route to improve conjugated polymer mechanical performance (DPP-Amide), but the intermolecular interactions must be carefully appraised as they may also be detrimental to device performance (DPP-Urea).

Experimental Methods

Materials

DPP-TVT based polymers were synthesized as previously described.[47] Nuclear magnetic resonance (NMR) spectra were recorded on a Bruker 300 MHz with variable temperature controller and are available in the SI (Figures S10-S12). Spectra for polymers were obtained in deuterated 1,1,2,2-tetrachlotoethane (TCE-d_2) at 120°C. High temperature GPC at 160°C, with trichlorobenzene as the eluent, was utilized to obtain the molecular weight and distribution of the polymers. Poly(sodium 4-styrenesulfonic acid) (PSS) was obtained from Sigma-Aldrich at a molecular weight of 75 kDa in 18% by volume aqueous solution and diluted to 3% for spin casting.

Film Preparation

All polymers were dissolved at 7 mg/ml in chlorobenzene at 80 °C overnight. For all measurements, the polymer solution was spun cast at 2000 rpm for a minimum of 2 minutes onto plasma treated silicon wafer.

Pseudo-Free-Standing Tensile Test

Uniaxial tensile tests were performed on top of a supporting water bath as described in our previous publication.[48] Composite films were first created by spin coating the polymer solution onto a sacrificial PSS layer. The PSS layer was formed by spin coating at 4000 rpm for 2 min. The composite films were then laser etched into dogbone geometries with a gauge width of 2 mm and length of 8 mm. Individually, the dogbones were dipped into water, dissolving the PSS sacrificial layer, and subsequently attached to a linear stage and load cell. A strain rate of $5*10^{-4}s^{-1}$ was then applied until the film broke. Force data was collected at a frequency of 10 Hz.

Free-standing Tensile Test

Uniaxial tensile tests were performed in air via the SMART technique as described in our previous publication.[36] A composite film is laser etched into a dogbone geometry (4 mm long, 2 mm wide) with an outer film support connected by etched microfibers. The composite film is then loaded onto a motorized stage at which water is deposited at the parameter of the film causing the PSS layer to dissolve and lift the film of interest. The film is then connected to the linear stage and load cell followed by translation of the

motorized stage at 0.15 mm/s. This enables the film to be sheared from the water surface and into an air environment. The side supports are then removed, and the film is ready for the tensile measurement. This was performed at the same strain rate as previously described.

Ellipsometry Characterization

Ellipsometry was performed with a M-2000® UI Ellipsometer from J.A. Woollam. Dry films were measured from 55°-75° at increments of 5°. Each angle was scanned for 2 seconds with a wavelength range from 245-1700 nm. To assist in the model development each film was spun cast onto a thermal oxide layer of ~500 nm to provide interference enhancement for increased sensitivity to absorbing films.[49,50] The oxide layer was measured prior to spin coating to ensure an accurate thickness of each layer. The data was modeled in CompleteEase software package. The samples were initially modeled using an anisotropic B-spline to establish a reference model. The B-spline was then converted to a series of gaussian oscillators (Gen-Osc) to minimize the number of variables required to fit the data and thus obtain an accurate assessment of the film optical constants and thickness. In the case of the composite films for tensile testing, the PSS layer was first measured followed by the composite film. The PSS layer was modeled using an isotropic Gen-Osc model. Thus, the model for the composite film uses known thickness from the PSS layer and allows for facile calculation of the thickness of the active polymer layer.

The *in-situ* film swelling experiments were performed at 23°C using a 500µL variable temperature liquid cell at a fixed incidence beam angle of 70°. The modeled wavelength range was reduced to 245-1100 nm due to the absorption of water in the infrared regime. Given this reduced spectral range, each film was spun cast onto a thermal oxide layer of known thickness for the swelling measurement. The films were exposed to de-ionized water for a period of 24 hours and measured every 2 seconds. The H_2O Pribil (temperature library) material file provided in the CompleteEase software package was used to model the ambient environment. Less than 20 parameters were allowed to vary with time to appropriately model the data yielding excellent fidelity.

Temperature dependent ellipsometry measurements were performed using a Linkam heat cell at an incidence angle of 70° while under a nitrogen atmosphere. Unlike the swelling measurements, the full spectral range (245-1700 nm) is assessable with the heat cell to increase model fidelity. Each polymer was heated to 300°C to remove thermal history from spin coating and subsequently cooled to -25°C at a rate of 5°C/min. The data was fitted with the previously described GEN-Osc models along with a material file of the silicon substrate and thermal oxide layer with known optical constants across the temperature profile. The oxide thickness was held constant. This helps to ensure accurate modeling of the film of interest as the optical constants of the substrate and interference oxide layer were already accounted for. The T_g was obtained from the cooling ramp based on the change in slope of the thickness dependence on temperature.

GIWAXS

GIWAXS was performed using a Xenocs Xeuss 2.0 SAXS/WAXS lab source instrument. All samples were exposed under vacuum for 2 hours with an incident beam energy of 8.05 keV, an incident angle of 0.2°and a beam geometry of 0.8 × 1.2 mm. The sample-to-detector distance was approximately 154 mm as determined by fitting a silver behenate standard. The 1D data and peak fitting were processed using Nika and WAXS tools software packages within Igor Pro from Wavemetrics.

Strain Dependent Charge Transport

Conjugated polymer semiconductors were processed through transfer printing according to the method described by Bao and co-workers.[9] First, the polymer inks were spun cast onto octadecyltrimethoxysilane (OTMS)-modified silicon wafers[41] and annealed at 150°C for 10 minutes in a nitrogen filled glovebox with <0.5 ppm of both O_2 and H_2O. Next, the annealed films were transferred onto a rectangular slab of poly(dimethylsiloxane) (PDMS) elastomer (base: crosslinker ratio = 20:1 w/w, crosslinked overnight at 70 °C in an oven). Each transferred film was stretched to a particular strain between 0-75% and subsequently transferred back to a p^+-doped 300 nm SiO_2 OTMS-modified wafer. Following film transfer, 50 nm of top contact Au source and drain electrodes were evaporated onto the wafers through a stencil shadow mask with 100 µm channel length and 1000 µm channel width oriented both parallel and perpendicular to the strain direction. The completed devices were then brought into the glovebox for testing with a Keithley 4200-SCS analyzer. Mobility calculations were performed in the saturation regime through linear fitting of the square root of drain current vs gate voltage, and inputting into the equation $\mu_{sat} = 2L/CW\ (\delta(I_D)^{1/2}/\delta V_G)^2$.

ASSOCIATED CONTENT

Supporting Information. Thin film mechanics, ellipsometry data, GIWAXS data, charge transport data, material synthesis, and NMR data.

AUTHOR INFORMATION

Corresponding Author

* Xiaodan Gu

Email: xiaodan.gu@usm.edu

* Simon Rondeau-Gagné

Email: simon.rondeau-gagne@uwindsor.ca

Author Contributions

L.A.G. and M.U.O. wrote the manuscript. L.A.G. characterized the mechanical, swelling, crystalline, and thermal behavior of

the polymers. M.U.O. synthesized and purified the polymers and performed OFET and COS characterization. Z.C.A. assisted in the GIWAXS characterization. S.R.-G. and X.G. coordinated the synthesis and characterization of these polymers, respectively. All authors have given approval to the final version of the manuscript.

Notes

The authors declare no competing financial interest.

ACKNOWLEDGMENT

We thank National Science Foundation under ward number DMR-2047689 for supporting this work. M.U.O thanks NSERC for support through a post-graduate doctoral scholarship (PGSD3-534870-19). S.R.-G. thanks the National Science and Engineering Research Council of Canada (NSERC) for financial support through a Discovery Grant (RGPIN-2017-06611).

REFERENCES

1. Rim, Y. S., Bae, S. H., Chen, H., De Marco, N. & Yang, Y. Recent Progress in Materials and Devices toward Printable and Flexible Sensors. *Adv. Mater.* **28**, 4415–4440 (2016).

2. Shih, C. C., Lee, W. Y., Lu, C., Wu, H. C. & Chen, W. C. Enhancing the Mechanical Durability of an Organic Field Effect Transistor through a Fluoroelastomer Substrate with a Crosslinking-Induced Self-Wrinkled Structure. *Adv. Electron. Mater.* **3**, 1–8 (2017).

3. Dang, W. *et al.* Flexible and Printed Electronics Stretchable electronics: recent progress in the preparation of stretchable and self-healing semiconducting conjugated polymers Related content Multiscale assembly of solution-processed organic electronics: the critical rol. *Flex. Print. Electron* **2**, 43002 (2017).

4. Galant, O., Bae, S., Silberstein, M. N. & Diesendruck, C. E. Highly Stretchable Polymers: Mechanical Properties Improvement by Balancing Intra- and Intermolecular Interactions. *Adv. Funct. Mater.* **30**, 1–8 (2020).

5. Hammock, M. L., Chortos, A., Tee, B. C. K., Tok, J. B. H. & Bao, Z. 25th Anniversary Article: The Evolution of Electronic Skin (E-Skin): A Brief History, Design Considerations, and Recent Progress. *Adv. Mater.* **25**, 5997–6038 (2013).

6. Root, S. E., Savagatrup, S., Printz, A. D., Rodriquez, D. & Lipomi, D. J. Mechanical Properties of Organic Semiconductors for Stretchable, Highly Flexible, and Mechanically Robust Electronics. *Chem. Rev.* **117**, 6467–6499 (2017).

7. Wang, G.-J. N., Gasperini, A. & Bao, Z. Stretchable Polymer Semiconductors for Plastic Electronics. *Adv. Electron. Mater.* **4**, 1700429 (2018).

8. Takamatsu, T., Chen, Y., Yoshimasu, T., Nishizawa, M. & Miyake, T. Bioelectronics: Highly Efficient, Flexible Wireless-Powered Circuit Printed on a Moist, Soft Contact Lens (Adv. Mater. Technol. 5/2019). *Adv. Mater. Technol.* doi:10.1002/admt.201970026.

9. Rivnay, J., Owens, R. M. & Malliaras, G. G. The rise of organic bioelectronics. *Chem. Mater.* **26**, 679–685 (2014).

10. Gubbi, J., Buyya, R., Marusic, S. & Palaniswami, M. Internet of Things (IoT): A vision, architectural elements, and future directions. *Futur. Gener. Comput. Syst.* **29**, 1645–1660 (2013).

11. Zhan, Y., Mei, Y. & Zheng, L. Materials capability and device performance in flexible electronics for the Internet of Things. *J. Mater. Chem. C* **2**, 1220–1232 (2014).

12. Wu, H. C. *et al.* A rapid and facile soft contact lamination method: Evaluation of polymer semiconductors for stretchable transistors. *Chem. Mater.* **26**, 4544–4551 (2014).

13. Li, Y. *et al.* An indacenodithiophene-based semiconducting polymer with high ductility for stretchable organic electronics. *Polym. Chem.* **8**, 5185–5193 (2017).

14. Savagatrup, S., Makaram, A. S., Burke, D. J. & Lipomi, D. J. Mechanical Properties of Conjugated Polymers and Polymer-Fullerene Composites as a Function of Molecular Structure. *Adv. Funct. Mater.* **24**, 1169–1181 (2014).

15. Choi, D. *et al.* Elastomer-Polymer Semiconductor Blends for High-Performance Stretchable Charge Transport Networks. *Chem. Mater.* **28**, 1196–1204 (2016).

16. Selivanova, M. *et al.* Morphology and Electronic Properties of Semiconducting Polymer and Branched Polyethylene Blends. *ACS Appl. Mater. Interfaces* (2019) doi:10.1021/acsami.8b22746.

17. Xu, J. *et al.* Highly Stretchable Polymer Semiconductor Films Through the Nanoconfinement Effect. *Science (80-.).* **355**, 59–64 (2017).

18. Zhang, S. *et al.* Tacky Elastomers to Enable Tear-Resistant and Autonomous Self-Healing Semiconductor Composites. *Adv. Funct. Mater.* **30**, 2000663 (2020).

19. Xu, J. *et al.* Multi-scale ordering in highly stretchable polymer semiconducting films. *Nat. Mater.* **18**, 594–601 (2019).

20. Oh, J. Y. *et al.* Stretchable self-healable semiconducting polymer film for active-matrix strain-sensing array. *Sci. Adv.* **5**, eaav3097 (2019).

21. Savagatrup, S., Zhao, X., Chan, E., Mei, J. & Lipomi, D. J. Effect of Broken Conjugation on the Stretchability of Semiconducting Polymers. *Macromol. Rapid Commun.* **37**, 1623–1628 (2016).

22. Bronstein, H., Nielsen, C. B., Schroeder, B. C. &

McCulloch, I. The role of chemical design in the performance of organic semiconductors. *Nat. Rev. Chem.* **4**, 66–77 (2020).

23. Savagatrup, S., Printz, A. D., O'Connor, T. F., Zaretski, A. V. & Lipomi, D. J. Molecularly stretchable electronics. *Chem. Mater.* **26**, 3028–3041 (2014).

24. Galuska, L. A. *et al.* Impact of Backbone Rigidity on the Thermomechanical Properties of Semiconducting Polymers with Conjugation Break Spacers. *Macromolecules* **53**, 6032–6042 (2020).

25. Yu, Z., Niu, X., Liu, Z. & Pei, Q. Intrinsically stretchable polymer light-emitting devices using carbon nanotube-polymer composite electrodes. *Adv. Mater.* **23**, 3989–3994 (2011).

26. Gasperini, A. *et al.* Characterization of Hydrogen Bonding Formation and Breaking in Semiconducting Polymers under Mechanical Strain. *Macromolecules* **52**, 2476–2486 (2019).

27. Yao, J. *et al.* Significant Improvement of Semiconducting Performance of the Diketopyrrolopyrrole–Quaterthiophene Conjugated Polymer through Side-Chain Engineering via Hydrogen-Bonding. *J. Am. Chem. Soc.* **138**, 173–185 (2016).

28. Ocheje, M. U. *et al.* Precise Control of Noncovalent Interactions in Semiconducting Polymers for High-Performance Organic Field-Effect Transistors. *Chem. Mater.* acs.chemmater.1c02426 (2021) doi:10.1021/acs.chemmater.1c02426.

29. Zhang, S., Galuska, L. A. & Gu, X. Water-assisted mechanical testing of polymeric thin-films. *J. Polym. Sci.* pol.20210281 (2021) doi:10.1002/pol.20210281.

30. Son, S. Y. *et al.* High-Field-Effect Mobility of Low-Crystallinity Conjugated Polymers with Localized Aggregates. *J. Am. Chem. Soc.* **138**, 8096–8103 (2016).

31. Kim, J.-S. *et al.* Tuning Mechanical and Optoelectrical Properties of Poly(3-hexylthiophene) through Systematic Regioregularity Control. *Macromolecules* **48**, 4339–4346 (2015).

32. Printz, A. D., Savagatrup, S., Burke, D. J., Purdy, T. N. & Lipomi, D. J. Increased elasticity of a low-bandgap conjugated copolymer by random segmentation for mechanically robust solar cells. *RSC Adv.* **4**, 13635–13643 (2014).

33. Ocheje, M. U. *et al.* Influence of amide-containing side chains on the mechanical properties of diketopyrrolopyrrole-based polymers. *Polym. Chem.* **9**, 5531–5542 (2018).

34. Zhang, S. *et al.* Toward the Prediction and Control of Glass Transition Temperature for Donor–Acceptor Polymers. *Adv. Funct. Mater.* **30**, 2002221 (2020).

35. Yılgör, E. Hydrogen bonding: a critical parameter in designing silicone copolymers. *Polymer (Guildf).* **42**, 7953–7959 (2001).

36. Galuska, L. A. *et al.* SMART transfer method to directly compare the mechanical response of water-supported and free-standing ultrathin polymeric films. *Nat. Commun.* **12**, 2347 (2021).

37. Bay, R. K. & Crosby, A. J. Uniaxial Extension of Ultrathin Freestanding Polymer Films. *ACS Macro Lett.* **8**, 1080–1085 (2019).

38. Campoy-Quiles, M., Etchegoin, P. G. & Bradley, D. D. C. On the optical anisotropy of conjugated polymer thin films. *Phys. Rev. B* **72**, 045209 (2005).

39. Lee, C., Stahlberg, E. A. & Fitzgerald, G. Chemical Structure of Urea in Water. *J. Phys. Chem.* **99**, 17737–17741 (1995).

40. Baker, J. L. *et al.* Quantification of Thin Film Crystallographic Orientation Using X-ray Diffraction with an Area Detector. *Langmuir* **26**, 9146–9151 (2010).

41. Rivnay, J., Mannsfeld, S. C. B., Miller, C. E., Salleo, A. & Toney, M. F. Quantitative Determination of Organic Semiconductor Microstructure from the Molecular to Device Scale. *Chem. Rev.* **112**, 5488–5519 (2012).

42. Sugiyama, F. *et al.* Effects of flexibility and branching of side chains on the mechanical properties of low-bandgap conjugated polymers. *Polym. Chem.* **9**, 4354–4363 (2018).

43. Zhang, S. *et al.* The Critical Role of Electron-Donating Thiophene Groups on the Mechanical and Thermal Properties of Donor–Acceptor Semiconducting Polymers. *Adv. Electron. Mater.* **5**, 1800899 (2019).

44. Keddie, J. L., Jones, R. A. L. & Cory, R. A. Size-Dependent Depression of the Glass Transition Temperature in Polymer Films. *Europhys. Lett.* **27**, 59–64 (1994).

45. Qian, Z. *et al.* Glass Transition Phenomenon for Conjugated Polymers. *Macromol. Chem. Phys.* **220**, 1900062 (2019).

46. Hajduk, B., Bednarski, H. & Trzebicka, B. Temperature-Dependent Spectroscopic Ellipsometry of Thin Polymer Films. *J. Phys. Chem. B* **124**, 3229–3251 (2020).

47. Ocheje, M. U. *et al.* Amide-Containing Alkyl Chains in Conjugated Polymers: Effect on Self-Assembly and Electronic Properties. *Macromolecules* **51**, 1336–1344 (2018).

48. Zhang, S. *et al.* Probing the Viscoelastic Property of Pseudo Free-Standing Conjugated Polymeric Thin Films. *Macromol. Rapid Commun.* **39**, 1800092 (2018).

49. McGahan, W. A., Johs, B. & Woollam, J. A. Techniques for ellipsometric measurement of the thickness and optical constants of thin absorbing films. *Thin Solid*

Films **234**, 443–446 (1993).

50. Campoy-Quiles, M., Alonso, M. I., Bradley, D. D. C. & Richter, L. J. Advanced Ellipsometric Characterization of Conjugated Polymer Films. *Adv. Funct. Mater.* **24**, 2116–2134 (2014).